Electric Power Systems Research 81 (2011) 1299–1307

Contents lists available at ScienceDirect

Electric Power Systems Research

journal homepage: www.elsevier.com/locate/epsr

Integration of a hybrid fuel cell-battery system to a distribution grid

Christina N. Papadimitriou*, Nicholas A. Vovos

University of Patras, Department of Electrical and Computer Engineering, Power Systems Laboratory, 26500 Rion, Greece

ARTICLE INFO

Article history:
Received 9 November 2009
Received in revised form
29 December 2010
Accepted 29 January 2011
Available online 24 February 2011

Keywords:
Distributed generation
Frequency control
Fuel cells
Fuzzy logic
Voltage control

ABSTRACT

In order to integrate a proton exchange membrane type (PEM) fuel cell system (FCS) combined with a battery bank to a distribution grid; this paper proposes a local controller based on fuzzy logic. The proposed system provides primary frequency control and local bus voltage support to the local grid. This opposes the passive distributed generation of the present that do not provide auxiliary services, such as back-up power, voltage support and reliability of supply as they operate under constant power factor equal to 1 at all times. During network disturbances, the distributed generations of the present are disconnected until normal operation is reestablished. When the distributed generation penetration is high this may lead to system instability. The microgrid concept is the effective solution for the control and quality improvement of grids with high level of DG penetration. So, the proposed system, also, can be an active controllable microsource of a microgrid in the future that cooperates with other microsources in order to cover the local load demands for active and reactive power either under grid-connected mode or under islanding operating mode. In cases where the distribution grid (working as microgrid) is forced to operate in islanded mode, the hybrid system provides the demanded active and reactive power. The FCS is connected to a weak distribution grid so that the system performance is studied under the worst conditions. The simulation results are obtained using MATLAB software under a severe step load change where the grid is still connected and under islanded operation. In both cases the system presents a good performance.

1. Introduction

In the next decade the penetration of distributed generation (DG) in the distribution grid is expected to play an important role in the power generation. Until now, penetration of DG in conventional systems is limited so that the systems overcome emergency situations with the usual procedure followed by the traditional Power Systems. Also, in weak distribution grids high DG penetration results in voltage rise problems, as thoroughly explained in [1], due to the distribution system operator (DSO) policy for DG to "fit and forget" requiring only operation at a fixed power factor. This policy fails to integrate the DG to the system and exploit its capability to mitigate such effects. Also, under remote fault conditions the DG is disconnected until the system recovers, due to safety concerns and the risks associated with an islanded system [2,3]. It is a strong belief, though, that DG in the form of one independent unit or in the form of a cluster of cooperating units (microgrid) can provide ancillary services such as reserves and voltage support under local disturbances and also play a significant role in islanded operation, providing the demanded active and reactive power by the critical loads. This can be achieved by the control of the DGs electronic interface to the main grid and the energy storage plants.

Efforts have been made in the past so that DG contributes in primary frequency control [4,5]. In Ref. [4], a FCS without a reformer is initially trying to supply demand power and in a second case a FCS with a reformer is combined with wind turbines that compensate the slow response of the FCS, trying to attain power equilibrium. The FCS has slow response, whether a reformer exists or not mainly because of the time delay of the system supplying air and the manifold dynamics. In Refs. [6,7], hybrid systems of fuel cell-battery have been presented and efforts have been made in order to regulate the fuel cell and the battery bank power to the dc side demand. In these cases, the hybrid systems operate in stand-alone mode without interfacing with an ac system.

In order to integrate DG to the grid, this paper proposes a fuzzy based local controller for a proton exchange membrane type (PEM) fuel cell system (FCS) combined with a battery bank providing primary frequency control and local bus voltage support. Under this operating philosophy, DG must support the grid during local distur-

Abbreviations: PEM, proton exchange membrane (fuel cell type); FCS, fuel cell system; DG, distributed generation; DSO, distribution system operator; MC, microsource controller; MGCC, microgrid central controller; DMS, distribution management systems; PCC, point of common coupling; MFs, membership functions; VSI, voltage source inverters; Fcs1–5, fuzzy controllers 1–5; IGBT, insulated gate bipolar junction transistor; PWM, pulse width modulation; PI, proportional integral; SCC, short circuit capacity.

* Corresponding author. Tel.: +30 210 6423465; fax: +30 2106423465.
E-mail addresses: chpapad@upatras.gr, chpapanetwork@gmail.com (C.N. Papadimitriou).

0378-7796/$ – see front matter © 2011 Elsevier B.V. All rights reserved.
doi:10.1016/j.epsr.2011.01.017

bances, as central generation supports high voltage systems in the transient period. In the control scheme presented here the hybrid system power covers both the ac and dc side power demand. This is because the FCS has been designed to operate both when the distribution system is connected to the mean voltage level of the grid and when it is disconnected from the grid and operates in stand-alone mode (as a part of a microgrid in the future). The microgrid concept is the effective solution for the control of grids with high level of DG penetration. The majority of the DGs comprising a microgrid are also controllable. So, in order to achieve the full benefits from the operation of the controllable distributed generation, a hierarchical control system architecture comprising three control levels can be envisaged in a future microgrid. The microsource controller (MC) uses local information to control the voltage and the frequency of the microgrid in transient conditions. The microgrid central controller (MGCC) optimizes the microgrid operation and the distribution management systems (DMS) optimizes multiple MGCC which are interfaced in. As the proposed controller in this paper is based on local information it will comprise the first layer MC of the FCS-battery system in the future microgrid. The battery bank delivers power only in the transient period and in steady state the FCS provides the overall power needed. The control has been designed to provide the system either partially with the demanded active and reactive power in case of a load change in grid-connected mode or the whole demanded energy in case of grid disconnection. The latter happens either due to a remote fault that has taken place at the mean voltage side or because the islanding operation mode is desirable for microgrids in some cases. After the fault is cleared the controller synchronizes the FCS with the main grid and the electrical connection is restored. In order to study the worst-case scenario, it is assumed that the point of common coupling (PCC) that the hybrid system is connected to, through a line to the distribution grid has low short circuit capacity. The system configuration is similar to this of a microgrid. So, a satisfactory operation of the hybrid system reassures its successful integration into a microgrid in the future. The response of the system is simulated firstly under a severe step load change under grid connected mode and secondly when a change to islanded operation mode is caused by an upstream supply outage, using MATLAB software. It is expected that in steady state the DSO should coordinate DG to optimize operation minimizing active power losses and maintaining flat voltage profile.

In the following section, the proposed hybrid system is described and analyzed. In Section 3 the local controller and its components are analyzed thoroughly. The simulation results are obtained and analyzed in Section 4. In Section 5, a study about the active power and voltage magnitude interaction is presented and the last section concludes the paper.

2. System description and modeling

The configuration of the system is shown in Fig. 1. The hybrid system of this study is consisted of a proton exchange membrane type (PEM) fuel cell system (FCS) and a battery bank. The adopted mathematical model of the FCS is fitted to this paper requirements. The FCS includes the following four main flow systems that are responsible for four main transient phenomena:

1. Hydrogen supply system to the anode
2. Air supply system to the cathode
3. De-ionized water as a coolant
4. De-ionized water to the humidifier of the membrane.

It is assumed in our study that for the first flow system a compressed hydrogen tank is available and that the hydrogen flow in the anode is adjusted according to the air flow in the cathode through a valve. For the second flow system, the "Chopper 2" (Fig. 1) controls the supplied dc power to a dc motor that drives a compressor which controls the air flow in the cathode. Therefore the rate of change of the power at the output of the FCS is limited by the overall inertia of the compressor and the motor. In our case, the study period of the system lasts for a few seconds. So, for the third subsystem it is assumed that the temperature of the fuel cell stack remains constant (80 °C) as the thermal dynamics are very slow with a time constant of about 10^2 s. Different operation temperatures of the FC lead to different polarization curves. If a fuel cell operates at higher temperatures, the shape of the voltage/current density graphs changes. In particular, the initial fall in voltage as current is drawn from the cell is remarkably less and the graph is more linear. In addition, there may be a higher current density at which the voltage falls rapidly, as with lower-temperature cells. In order to determine the desired operation temperature the following is taken in mind: operating temperatures of over 60 °C are desirable because they reduce losses, especially when the cathode activation voltage drops. Also, it makes economic sense to operate the fuel cell at maximum possible power density, even if the extra weight, volume, cost, and complexity of the humidification system are taken into account. With larger cells, all these are proportionally less important. On the other hand, in real systems, it is very difficult to arrange proper FC humidification at temperatures above 80 °C unless the system is pressurized to about 2 bar or more or else the system will dry out. Typical operating temperature of a PEM type FC is 80 °C and this value is chosen as the initial temperature for the simulated FCS. About the fourth system, it is assumed that the membrane of the model is fully humidified as the membrane hydration has a transient phase of about 10 s [8]. It has to be mentioned, that the air flow dynamics and the humidity management define the FCS response. By assuming that the membrane is fully humidified, the designed controller for the second subsystem can be safely decoupled from the humidity. Also, the "double-layer charging effect" has been neglected taking into account that the time constant is merely 10^{-19} s [9]. The FCS is designed to be self-powered meaning that every auxiliary component of the FCS must be supplied by the FCS power particularly including the air supply system. At the output of the FCS, the "Chopper 1" is connected so that the dc voltage is boosted [10,11] and the FCS's output is regulated, without exceeding the FCS capabilities. The battery bank is connected in order to support the dc voltage, to keep its deviations into certain limits and to support FCS's performance under fast load changes as FCS dynamics are slow. The hybrid system interfaces with the ac-side system through a voltage source inverter (VSI) so that the active and reactive power can be controlled independently. An L-C filter is located at the VSI output followed by a step-up transformer. The transformer is connected to the point of common coupling (PCC) with a 2 km distribution line where a passive load and an induction motor are connected at the low voltage side of the distribution grid.

3. Fuzzy local controller

The four main flow subsystems that were briefly mentioned in the previous section and the auxiliary subsystems that are beyond the scope of this paper, establish a non linear FCS. The non linearity of the system and some key points of great significance for the system efficiency and performance are outlined below and justify the application of a fuzzy based intelligent control. Firstly, it is significant for the compressor motor controller (Chopper 2) to have a good dynamic response during fast load changes, so that the FCS voltage does not drop dramatically leading to oxygen starvation. Secondly, the "Chopper 1" controller has to act simultaneously

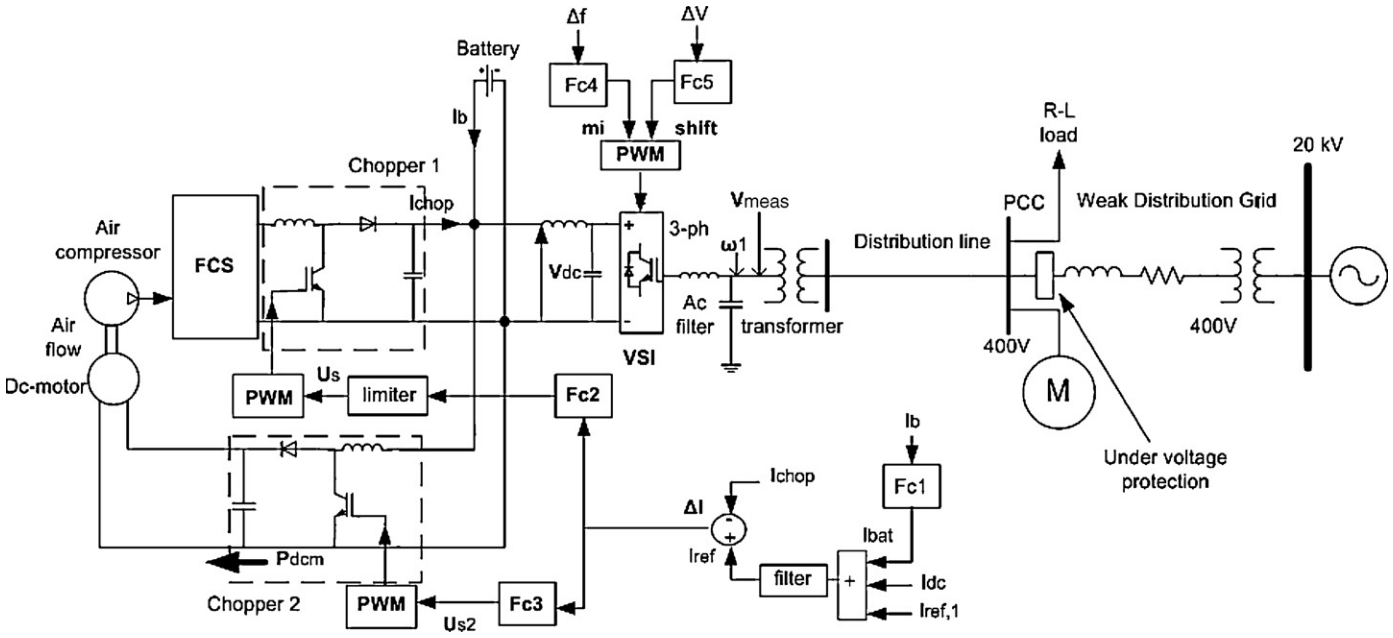

Fig. 1. Proposed hybrid system.

with the fuel flow control achieving stability and accuracy while minimizing overshooting and current rippling. The VSI controllers have to meet the same requirements too. Given that, the fuzzy logic seems an attractive proposal as it does not require a precise mathematical modeling or sophisticated computations that in many cases lack efficiency and good performance. The fuzzy logic controllers are non linear and adaptive in nature and thus it is expected to have a robust performance under disturbances.

The controllers force the hybrid system to provide primary frequency control and local bus voltage support under local disturbances. After a remote fault at the mean voltage side and after an upstream supply outage, the controllers force the hybrid system to provide the demanded active and reactive power to the loads at the PCC. The local controllers consist of 5 different fuzzy controllers (Fcs), Fig. 1. In Table 1 the input and the output signals of every fuzzy controller are given in symbols. The used symbols are explained briefly in the nomenclature. The signals are analyzed in details in the following subsections.

The fuzzy controllers are designed from a heuristic knowledge of the system. Of course, they are thoroughly iterated by system simulation study in order to be fine tuned. The advantage of this method is the fast convergence as it provides adaptively decreasing step size in the search of the adequate output. Besides, noisy and varying input signals do not affect the search. So, the weights of the membership functions (MFs) of every controller were chosen after qualitative knowledge of the simulation system. Triangular MFs were chosen as the most popular type providing satisfactory results. Some MFs, though, were chosen to have Gaussian shape in order to limit the output values to the desired and succeed better convergence. It can be seen that the MFs are asymmetrical, giving more sensitivity as the variables approach zero values.

Table 1
Inputs and outputs of the fuzzy controllers.

	Fcs1	Fcs2	Fcs3	Fcs4	Fcs5
Input	I_b	ΔI	ΔI	Δf	ΔV
Output	ΔI_{bat}	ΔU_s	ΔU_{s2}	Δm_i	$\Delta shift$

3.1. Chopper 1 control

The battery bank supports the FCS when fast transient phenomena occur as the FCS has slow dynamics and certain technical limitations. In steady state, the FCS of the study has to provide itself the whole demanded power, forces the current supplied by the battery bank to be zero and charges the battery bank if it is asked by the monitoring system. Depending on the battery size, the load demand that the battery is required to supply during the transient period and the battery state of charge, the battery voltage could reach the lower battery voltage limit. In this case a low voltage protection is applied and the transient FCS support to the distribution grid is cancelled. The Chopper 1 control includes the fuzzy controllers 1 and 2. The fuzzy controller 2 (Fc2) ensures through the duty cycle of Chopper 1 that the FCS provides the demanded power by the ac-side, the demanded power by the dc-motor and forces the current supplying by the battery bank to zero in steady-state. The reference current I_{ref} (Fig. 1) for this controller is the sum of three currents:

$$I_{ref} = I_{ref,1} + I_{dc} + I_{bat} \quad (1)$$

The first signal $I_{ref,1}$ is expressed by the following equation:

$$I_{ref,1} = \frac{P_o + \sum \Delta P}{V_{dc}} \quad (2)$$

where P_o is the steady state power value and

$\sum \Delta P$ the sum of the power variations according to a power droop, given by the following equation:

$$\Delta P = -k \times (\omega_1 - \omega_{ref}) \quad (3)$$

where

k: droop coefficient equal to 2 after tests in our study system.
ω_1: calculated value of frequency at the VSI output.
ω_{ref}: reference value of frequency.

The $I_{ref,1}$ current ensures that the active output power of the FCS fits the new demand of the distribution grid.

The second reference current I_{dc} is created according to the absorbed power of the dc motor and is expressed by the following

Table 2
Input and output of the Fc1.

Fc1 input	VP	MP	P	OK	NEG	MNEG	VNEG
Fc1 output	POS_H	POS_M	POS_L	OK	NEG_L	NEG_M	NEG_H

equation:

$$I_{dc} = \frac{P_{dcm}}{V_{dc}} \tag{4}$$

where P_{dcm} is the absorbed power of the dc motor and V_{dc} is the measured dc voltage at the battery output.

The I_{dc} ensures that the FCS covers the dc motor power.

The third sigal I_{bat} is created through the output of the Fc1 whose output values ΔI_{bat} are added together in every simulation step in order to comprise the I_{bat} value at the steady state according to the following equation:

$$I_{bat}^{n+1} = I_{bat}^{n} + \Delta I_{bat} \tag{5}$$

where I_{bat}^{n+1} is the new value of I_{bat} and I_{bat}^{n} is the old value of I_{bat}.

The input of Fc1 is the battery bank current I_b and ensures that the battery bank supplying current is forced to zero in steady state.

When I_b is positive the output of the Fc1 is positive and is added in order to build the I_{bat} signal. When I_b is negative, a negative output of Fc1 is added to the I_{bat} value. When the current of the battery bank is zero the I_{bat} has reached its steady state value. In steady state and when a charging of the battery bank is asked from the monitoring system, the reference I_{bat} takes a constant value equal to the charging current of the battery bank.

The error ΔI between the I_{ref} and the measured dc current at the output of chopper 1, I_{chop}, drives the Fc2. The output of the Fc2 is the deviations ΔU_s of the signal U_s. The sum of ΔU_s creates the U_s signal which determines the duty cycle of the Chopper 1, where the PWM is used [12]. This signal must not exceed the FCS capabilities and this is ensured by the limiter at the output of the Fc2.

$$U_s^{n+1} = U_s^{n} + \Delta U_s \tag{6}$$

where U_s^{n+1} is the new value of U_s and U_s^{n} is the old value of U_s.

When the I_{chop} value is lower than the reference signal value, the duty cycle of the chopper 1 augments. The opposite happens when the I_{chop} is greater than the reference value. The fuzzy variables of the inputs of the Fc1 and Fc2 are expressed by the following linguistic variables: "very very positive (VVP)" "very positive (VP)", "medium positive (MP)", "positive (P)", "negative (NEG)", "medium negative (MNEG)", "very negative (VNEG)", "very very negative (VVNEG)". The fuzzy variables of the outputs of the Fc4 and Fc5 are expressed by the following linguistic variables: "very high positive (POS_VH)", "high positive (POS_H)", "medium positive (POS_M)", "low positive (POS_L)", "very high negative (NEG_VH)", "high negative (NEG_H)", "medium negative (NEG_M)", "low negative (NEG_L)". The rules of the Fc1 and Fc2 are shown in Tables 2 and 3, respectively. Their membership functions are shown in Figs. 2–5.

3.2. Chopper 2 control

The fuzzy controller 3 (Fc3) constitutes the Chopper 2 control and determines through its duty ratio the power that the dc-motor of the FCS absorbs and therefore regulates the air flow supplied by the compressor to the FCS. According to the pressure variation of the supplied air, the supplied hydrogen from the hydrogen tank is regulated through a valve and this regulates the output power of the FCS according to the demanded power by the system without oxygen starvation. In our study, the hydrogen flow is regulated to the oxygen flow through a simple PI controller. The indication of an oxygen starvation is the excess oxygen ratio λ_{O2} which is the ratio of oxygen supplied to oxygen used in the cathode. The optimum value of λ_{O2} is taken equal to 2 where for our chosen FCS the net deliverable power is about maximum [9].

So, the input signal of the Fc3 is the same as in the Fc2. The output of the Fc3 is the deviations ΔU_{s2} of a signal U_{s2}, whose sum builds a signal used in the PWM method applied on the switch of the Chopper 2 and determines its duty cycle according to the following equation:

$$U_{s2}^{n+1} = U_{s2}^{n} + \Delta U_{s2} \tag{7}$$

where U_{s2}^{n+1} is the new value of U_{s2} and U_{s2}^{n} is the old value of U_{s2}.

When the I_{chop} value is lower than the reference signal value, the duty cycle of the chopper 2 augments and the air flow to the cathode augments too. The opposite happens when the I_{chop} is greater than the reference value. The rules of the controller are also the same as

Table 3
Input and output of the Fc2.

Fc2 input	VVP	VP	MP	P	OK	NEG	MNEG	VNEG	VVNEG
Fc2 output	POSVH	POSH	POSM	POSL	OK	NEGL	NEGM	NEGH	NEGVH

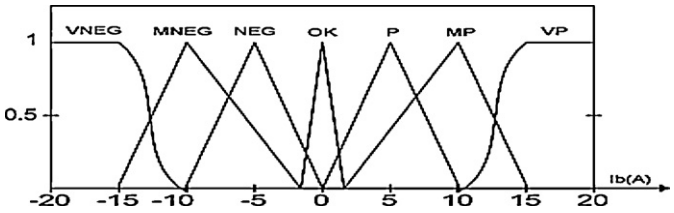

Fig. 2. Membership functions for the input signal of Fc1.

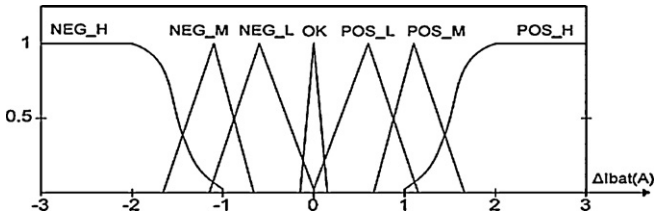

Fig. 3. Membership functions for the output signal of Fc1.

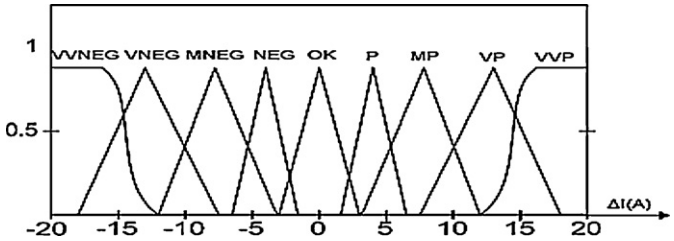

Fig. 4. Membership functions for the input signal of Fc2.

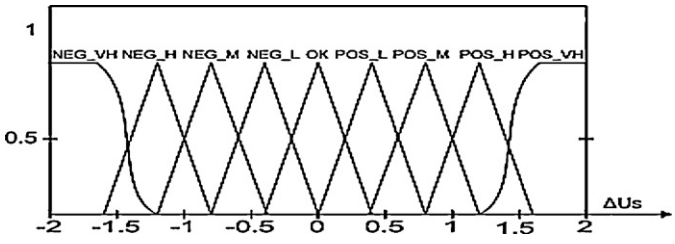

Fig. 5. Membership functions for the output signal of Fc2.

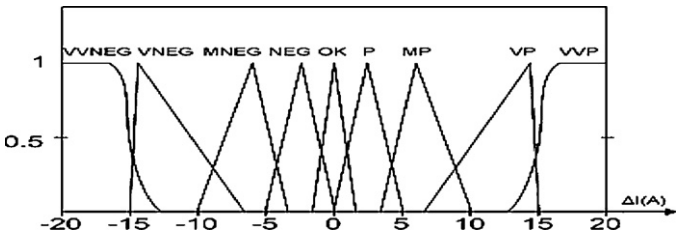

Fig. 6. Membership functions of the input signal of Fc3.

in Fc2 of chopper 1 but with different weights, resulted after tests in our system. The membership functions are also different and are shown in Figs. 6 and 7.

3.3. VSI control

The VSI control consists of the fuzzy controllers 4 and 5. The controllers 4 and 5 ensure through the IGBT's switching of the VSI that the hybrid system provides a part of the demanded active and reactive power by the ac side when a local disturbance occur or supplies the whole demanded power after the distribution grid is disconnected. After simulation tests in our system, the dependency of the voltage magnitude from the active power was found stronger than this from the reactive power. This happens as the distribution grid of our study is weak and has a low short circuit ratio 2 and the distribution line has a low X/R ratio 0.5 [13]. This issue is further analyzed in Section 5.

The control of the active power is achieved through the modulation index (m_i) of the PWM method. The value of m_i is determined by the output of the fuzzy controller 4 (Fc4) which is the deviations Δm_i of the modulation index signal whose values are added together in every simulation step in order to comprise the m_i value at steady state:

$$m_i^{n+1} = m_i^n + \Delta m_i \tag{8}$$

where m_i^{n+1} is the new value of m_i and m_i^n is the old value of m_i.

The input of this controller is the error between the measured frequency at the VSI output and the reference frequency value. This error is used in a droop Eq. (3) written in the previous section. When the measured frequency is lower than the reference value, the m_i value increases in order that the dc side supplies more active power. The opposite happens when the measured frequency is greater than the reference value. When the measured frequency equals to the reference value, the input and the output of the Fc4 becomes zero and the m_i has a constant value.

The control of the reactive power is achieved through the *shift* of the phase angle of the sinusoidal reference signal of the PWM method. The fuzzy controller 5 (Fc5) determines the *shift* value. The input of this controller is the error between the reference voltage and the measured voltage V_{meas} at the VSI output. Its output is the deviations $\Delta shift$ of the *shift* signal whose values are added together in every simulation step in order to comprise the *shift* value according to the following:

$$shift^{n+1} = shift^n + \Delta shift \tag{9}$$

where $shift^{n+1}$ is the new value of *shift* and $shift^n$ is the old value of *shift*.

When the measured voltage is lower than the reference value the *shift* increases and the opposite happens when the measured voltage is greater than the reference value. The *shift* value is constant when the error between the measured and the reference value of the voltage becomes equal to zero. The fuzzy variables of the inputs of the Fc4 and Fc5 are expressed by the following linguistic variables: "positive (POS)", "zero (OK)", "negative (NEG)". The fuzzy variables of the outputs of the Fc4 and Fc5 are expressed by the following linguistic variables: "high positive (POS_H)", "medium positive (POS_M)", "low positive (POS_L)", "high negative (NEG_H)", "medium negative (NEG_M)", "low negative (NEG_L)". The rules of the Fc4 and Fc5 are shown in Tables 4 and 5, respectively. Their membership functions are shown in Figs. 8–11.

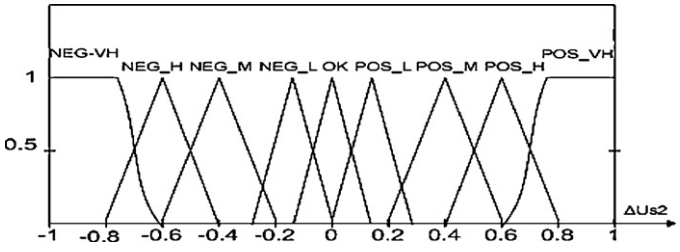

Fig. 7. Membership functions of the output signal of Fc3.

Table 4
Input and output of the Fc4.

Fc4 input	POS	POS	POS	OK	NEG	NEG	NEG
Fc4 output	NEG_H	NEG_M	NEG_L	OK	POS_L	POS_M	POS_H

Table 5
Input and output of the Fc5.

Fc5 input	POS	POS	POS	OK	NEG	NEG	NEG
Fc5 output	POS_H	POS_M	POS_L	OK	NEG_L	NEG_M	NEG_H

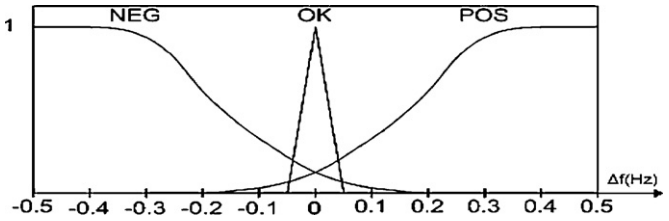

Fig. 8. Membership functions of the input signal of Fc4.

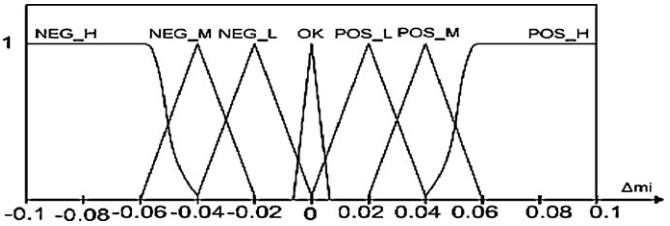

Fig. 9. Membership functions of the output signal of Fc4.

4. Simulation results

The data for the system of Fig. 1 are given in Appendix B. The power and voltage bases for the pu system are: 10 kW, 380 V,

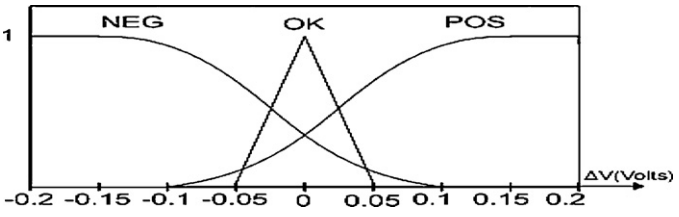

Fig. 10. Membership functions of the input signal of Fc5.

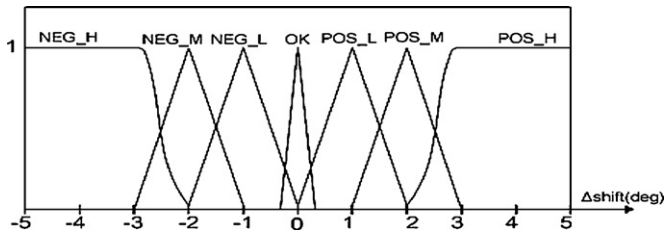

Fig. 11. Membership functions of the output signal of Fc5.

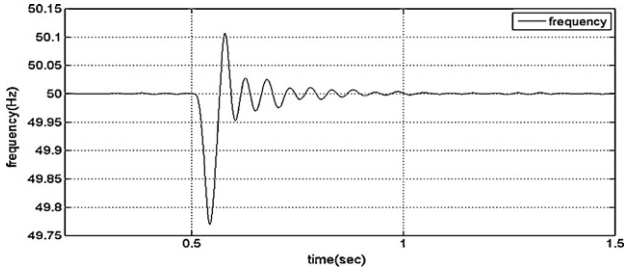

Fig. 12. The frequency at the VSI output.

respectively, also mentioned in the appendix. In Section 4.1 the control system response was tested under local disturbances in grid connected mode and in Section 4.2 the control system response was tested in islanded operation.

4.1. System performance under local disturbances in grid-connected mode

In steady state, the R-L load absorbs its nominal active and reactive power and the ac motor operates at a slip of 0.013 and absorbs 0.9 kW and 0.6 kVar. In steady state the grid feeds almost the 60% of the active power and the 100% of the reactive power of the loads. The rest 40% of the demanded active power is fed by the hybrid system.

At 0.5 s, a step load increase of the mechanical load of the inductive machine is imposed. The mechanical load is doubled and the hybrid system provides the ancillary services while the grid is still connected. Some representative results are shown in Figs. 12–17. In Figs. 12 and 13, at 0.5 s, the frequency and the voltage drop due to the unbalance of active and reactive powers in the system and returns to their nominal value after some oscillations within 0.5 s. In Fig. 14, the hybrid system provides the demanded active power forced by the VSI controller. It can be seen that the hybrid system supplies the 40% of the active power of the load. The rest 60% is supplied by the grid. In Fig. 15 the battery bank provides rapidly the demanded power and after 4 s the battery bank current is forced to zero. The FCS power is shown in Fig. 16. Initially, the FCS does not react as it has slow dynamics but it is slowly forced (due to technical limitations) to provide the demanded power within 4 s. In Fig. 17 the simulated current at Chopper 1 output and the current reference value are plotted in the same graph proving the good performance of Chopper 1 controller.

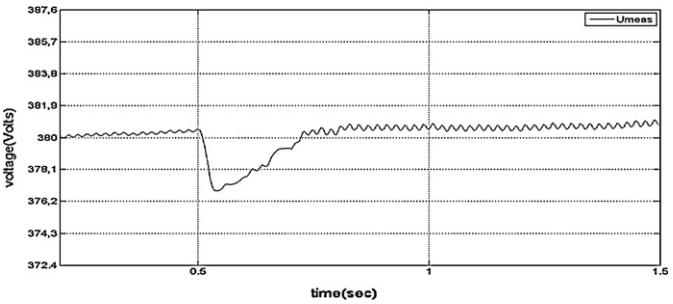

Fig. 13. The voltage at PCC in pu.

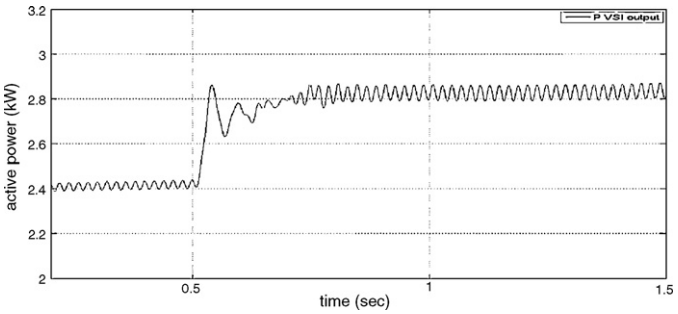

Fig. 14. The active power at the VSI output in pu.

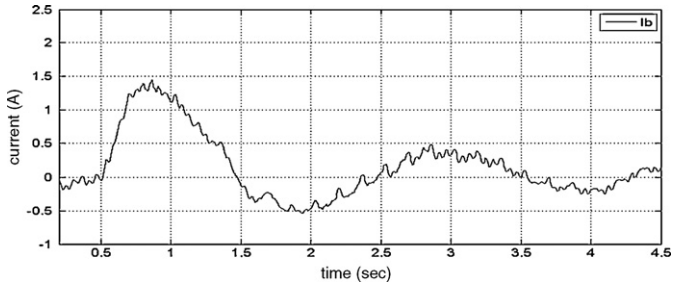

Fig. 15. The battery bank current in steady state and transient period.

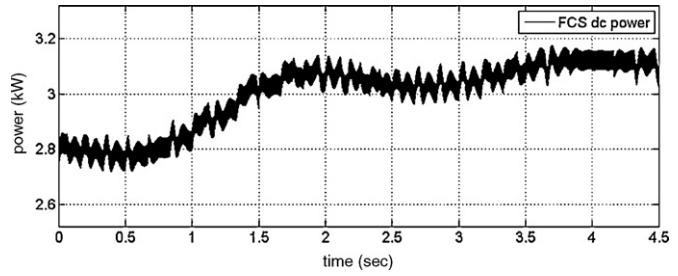

Fig. 16. The FCS delivered power.

4.2. System performance in islanded operation mode

The steady state of the system is the same as in the previous case. At 0.5 s, the distribution grid is disconnected after a fault at the mean voltage side and the hybrid system provides the ancillary services. Some representative results are shown in Figs. 18–23. In Fig. 18, at 0.5 s, the frequency drops and returns to its nominal value after some oscillations within 1.5 s. In Fig. 19, at 0.5 s, the volt-

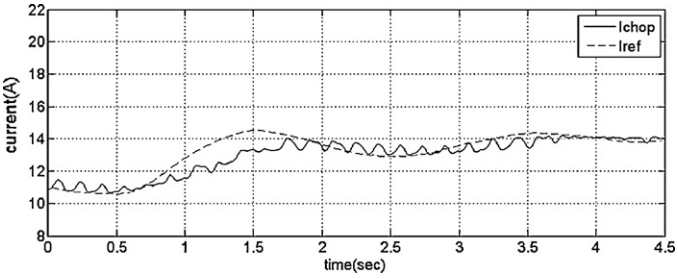

Fig. 17. The signals I_{chop} and the I_{ref} plotted in the same graph.

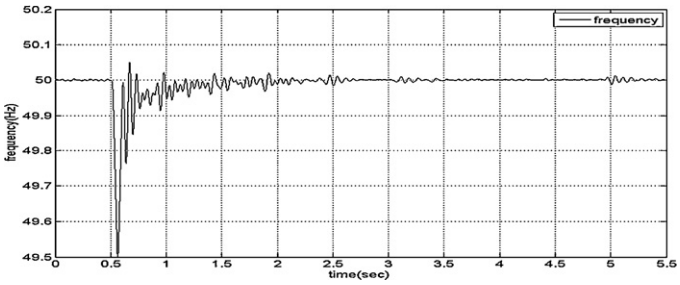

Fig. 18. The frequency at the VSI output.

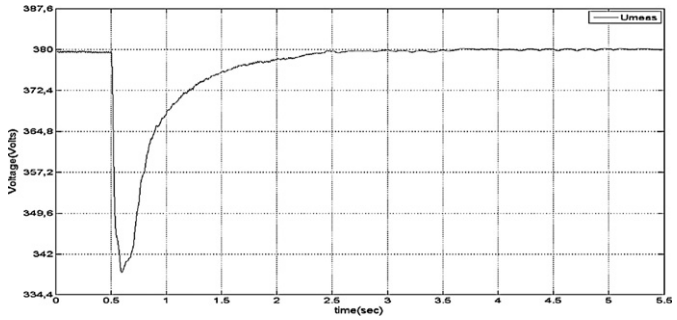

Fig. 19. The voltage at PCC in pu.

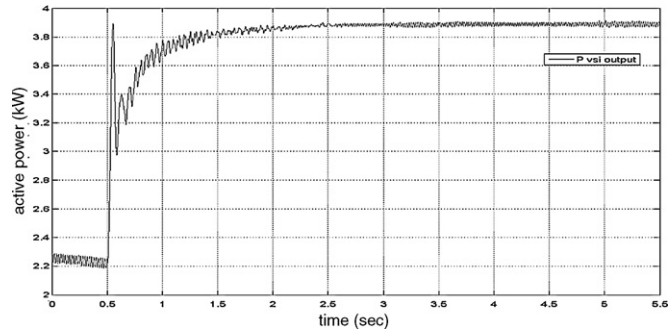

Fig. 20. The active power at the VSI output in pu.

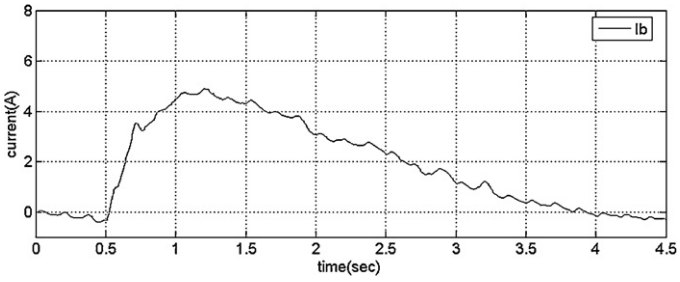

Fig. 21. The battery bank current in steady state and transient period.

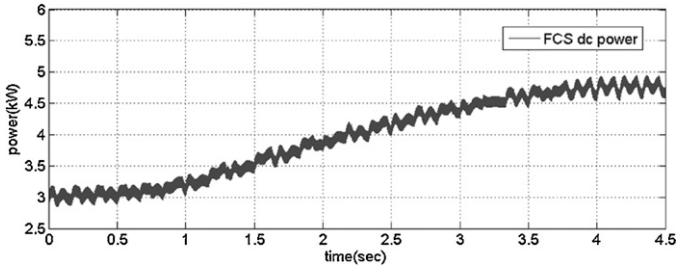

Fig. 22. The FCS delivered power.

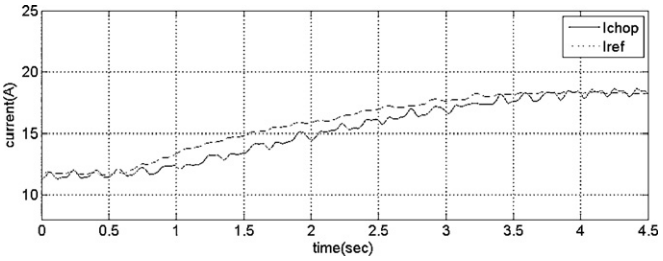

Fig. 23. The signals I_{chop} and the I_{ref} plotted in the same graph.

age drops and returns to its nominal value after some oscillations within 2 s. The drop for the signals of both frequency and voltage is greater than the drop of the same signals observed in the previous case (local disturbances) as the insufficiency of both active and reactive power is greater too.

In Fig. 20, the hybrid system provides the demanded active power forced by the VSI controller. In Fig. 21 the battery bank current increases rapidly in order that the battery bank supplies the demanded power and returns to zero within 4 s. In Fig. 22 the FCS provides the whole demanded active power within 4 s. In Fig. 23 the Chopper 1 controller performance proves good.

5. Active power and voltage magnitude interaction

It is well known that in the high voltage transmission systems the frequency is depended from the active power and the voltage from the reactive power. This happens as the high voltage grids appear strongly inductive behavior. On the contrary, in distribution systems the above dependency can be reversed and the voltage may be rather stronger depended from the active power and the frequency from the reactive power as they appear strongly resistive behavior. The relation among the mentioned quantities depends on the values of short circuit capacity (SCC) and the X/R ratio as they appear on a node of the grid. When the SCC and the X/R are low, the grid is strongly resistive and active power control through the voltage magnitude can be achieved. As the SCC and X/R ratio increases an interaction between the active and reactive control loops can be observed. When the SCC and the X/R are high, the grid is strongly inductive and active power control through the frequency can be achieved. After simulation tests in our system, an expected considerable interaction between the active and reactive control loops was observed. The dependency of the voltage magnitude from the active power is stronger than this from the reactive power. This is fully justified by the fact that the distribution grid of our study is weak with a low short circuit ratio 2 and the distribution line has a low X/R ratio 0.5 and therefore it appears a strongly resistive behavior.

Simulation tests with 3 distribution lines of different X/R ratios were made in the system that is already described in order to evaluate the control performance and to make some safe conclusions. For our tests we considered the parameters of 3 typical distribution lines of the Greek network of about 0.22, 0.5 and 0.85 X/R ratio. The length of each distribution line, 1.5 km, 2 km and 2.5 km, respectively, is chosen so that the SCC remains almost the same in every test case. This way the voltage drop at every line is almost the same too. The type and the parameters of the distribution lines are shown in Table 6.

The control performance was evaluated under two cases of study, the local disturbance occasion (the same as previous section) and the islanded operation. During the tests no changes or regulations were done to the fuzzy controllers. In order to evaluate the controller's response in each case the frequency and voltage of the simulated system at the VSI output are presented.

Table 6
Parameters of distribution lines.

		X (Ω/km)	R (Ω/km)	Length (km)
1	Cu & Al type ($4 \times 16\,mm^2$)	0.308	1.248	1.5
2	AAAC type ($4 \times 70\,mm^2$)	0.268	0.565	2
3	Cu & Al type ($4 \times 70\,mm^2$)	0.261	0.301	2.5

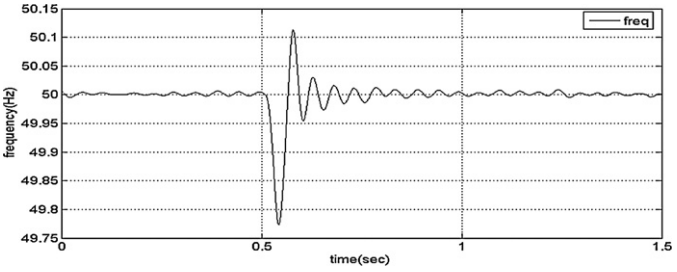

Fig. 24. The frequency at VSI output during local disturbance and in steady state.

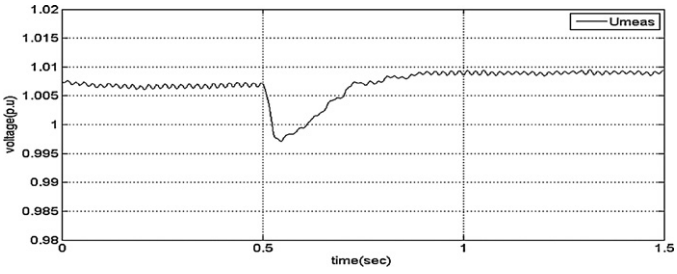

Fig. 25. The voltage at VSI output during local disturbance and in steady state.

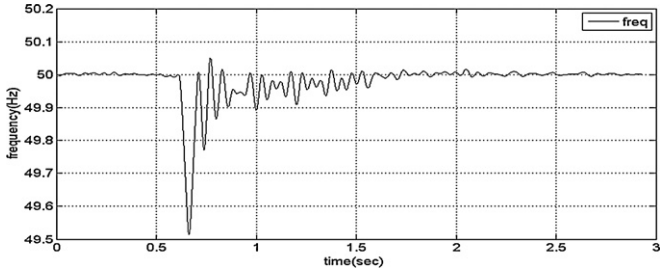

Fig. 26. The frequency at VSI output in islanded operation.

The control behavior revealed satisfactory in both cases of study for the first line of 0.22 X/R ratio as is presented in Figs. 24–27. In Figs. 24 and 25 the frequency and the voltage returns to their nominal values within 0.7 s after some oscillations. It is also observed an overshooting at the frequency signal that is acceptable. In Figs. 26 and 27 the grid is disconnected at 0.6 s and both the frequency and the voltage recover within 2.3 s. The behavior of the voltage signal in Fig. 27 at 1.5 s dictates that a regulation at the

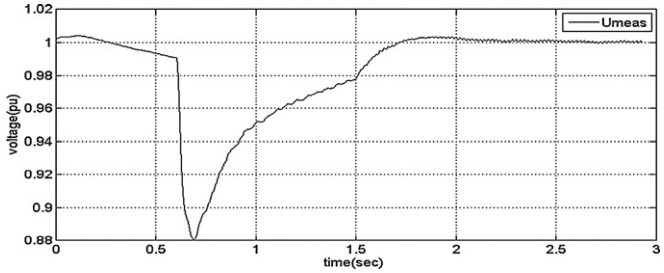

Fig. 27. The voltage at VSI output in islanded operation.

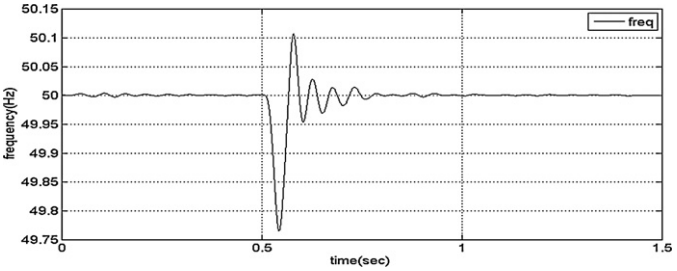

Fig. 28. The frequency at VSI output during local disturbance and in steady state.

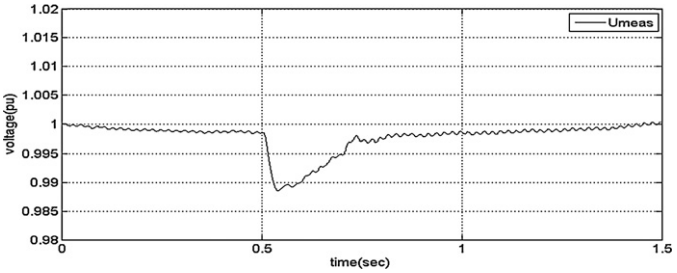

Fig. 29. The voltage at VSI output during local disturbance and in steady state.

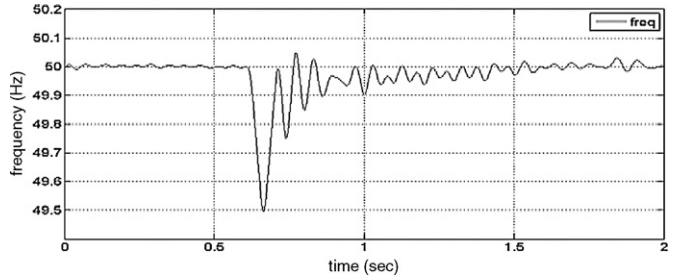

Fig. 30. The frequency at VSI output in islanded operation.

membership function of Fc1 and Fc5 should be done for better responses.

For the line of 0.5 X/R ratio the results have been already shown and analyzed in Figs. 12–13 and 18–19.

The control behavior revealed also satisfactory for the third line of 0.85 X/R ratio as is presented in Figs. 28–31. In Figs. 28 and 29 the frequency and the voltage return to their nominal values in about 0.7 s after some oscillations. In Figs. 30 and 31 the grid is disconnected at 0.6 s and both the frequency and the voltage recover within 1.3 s. The behavior of the signal in Fig. 31 at 1.4 s dictates that a regulation at the membership functions of Fc1 and Fc5 should be done for optimal results.

The X/R ratio in practical distribution lines does never exceeds the value of 1. Therefore, the proposed fuzzy controllers can perform satisfactorily for all the distribution grids.

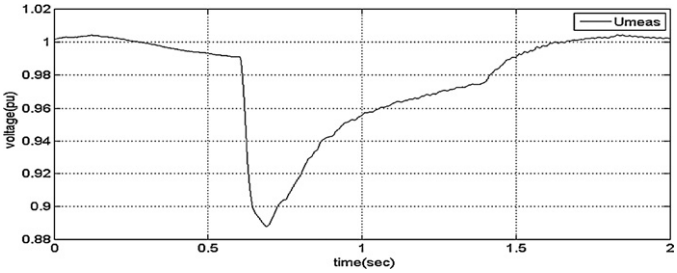

Fig. 31. The voltage at VSI output in islanded operation.

For theoretical purposes the controller was tested for two distribution lines of 2.5 and 3.5 X/R. At the value of 2.5 X/R, the controller performance deteriorates in both cases of study. At the value of 3.5 X/R, the controller can force the hybrid system to support the grid under small local disturbances. But, when the grid is disconnected after a remote fault at the mean voltage side, the control is unable to force the hybrid system to provide the demanded power. This happens because the dependency relation has dramatically changed and the active power control through the voltage magnitude becomes ineffective. In this section the effectiveness of the proposed local controller when the grid's behavior changes from resistive to inductive and vice versa was investigated. In practical cases, however, the behavior of a grid cannot change dramatically and the fuzzy controller revealed to perform well in a wide range of X/R. In the future, though, the fuzzy local controller could be designed to incorporate the reactive and active power loop interaction.

6. Conclusion

This paper proposes a controller based in fuzzy logic in order to integrate a hybrid system of fuel cell and battery bank into the distribution grid so as in the future this system could be incorporated in a cluster of cooperating and controllable DGs (microgrid). The hybrid system is evaluated under two disturbance cases: (a) local disturbances such as a severe step load change. (b) transition from the connected to islanded operation mode either after a remote fault at the mean voltage side or intentionally. The simulation results prove that the hybrid system can provide ancillary services at the distribution grid under both modes of operation. The system response was analyzed and revealed good performance. After the transient period, a coordination of the DG to optimize operation minimizing active power losses and maintaining flat voltage profile is suggested.

Acknowledgment

The authors thank the European Social Fund (ESF), Operational Program for EPEDVM and particularly the Program Herakleitos II, for financially supporting this work.

Appendix A. List of symbols

$I_{ref,1}$ reference created according to a power droop from the ac-side

ΔP, $\sum \Delta P$ deviations of the demanded active power from the ac-side and the sum of the demanded active power from the ac-side, respectively

k droop coefficient

ω_1 calculated value of frequency at the inerter output

ω_{ref} reference value of frequency

P_o steady state power value

V_{dc} measured voltage at the battery output

I_{dc} reference current created according to the absorbed power of the dc motor

P_{dcm} absorbed power of the dc motor

I_b the calculated current of the battery and input of Fc1

I_{bat}, ΔI_{bat} the output signal of the Fc1 and the deviations of this signal, respectively.

I_{ref} the total reference value of the dc current

I_{chop} calculated current at the output of the chopper 1

ΔI the error of the calculated current at the output the chopper 1 I_{chop} from its reference I_{ref}. It comprises the input of both Fc2 and Fc3

U_s, ΔU_s the signal that controls the duty cycle of the chopper 1 and the deviations of this signal (output of Fc2)

U_{s2},ΔU_{s2} the signal that controls the duty cycle of the Chopper 2 the deviations of this signal (output of Fc3)

λ_{O2} oxygen excess ratio

Δf the error of the calculated value of frequency at the inverter output from its reference value (input of Fc4)

m_i, Δm_i the modulation index signal of the PWM method and the change of this signal (output of Fc4), respectively

V_{meas}, ΔV the measured voltage at the point of common coupling and the error between the V_{meas} signal and its reference value (input of Fc5), respectively.

shift, Δ*shift* the signal of the PWM method and the change of the this signal (output of Fc5), respectively

Appendix B.

FCS PEM: 10 kW, 150 cells, 100 A, 100 V, 280 cm^2/cell
Distribution line: AAAC type (4×70), X (Ω/km) = 0.268, R (Ω/km) = 0.565, 2 km.
AC system: 380 V, 50 Hz, base pu:10 kW, 380 V.
R-L load: 3 kW, 1 kVar, 380 V
Induction motor: 2.4 hp, 400 V, 50 Hz, 1500 rpm
dc-motor: 1 hp, 300 V, 1750 rpm, field: 150 V
Battery bank: 210 HV nickel-metal hybrid cells of 1.2 V, 2 A h, 250 V
Transformer: 10 kVA, 170:380 V, 50 Hz

References

[1] C.L. Masters, Voltage rise: the big issue when connecting embedded generation to long 11 kV overhead lines, Inst. Elect. Eng. Power Eng. J. 16 (1) (2002) 5–12.
[2] R. Caldon, F. Rossetto, R. Turri, Temporary islanded operation of dispersed generation on distributed networks, in: Universities Power Engineering Conference, UPEC 2004, 39th International, vol. 3, 2004, pp. 987–991.
[3] X. Ding, P.A. Crossley, D.J. Morrow, Future distribution networks with distributed generation capable of operating in islanded mode, in: Universities Power Engineering Conference, UPEC 2004, 39th International, vol. 1, 2004, pp. 773–776.
[4] J. Morren, S.W.H. de Haan, J.A. Ferreira, Primary power/frequency control with wind turbines and fuel cells, in: Power Engineering Society General Meeting, IEEE, 2006, p. 8.
[5] J. Morren, S.W.H. de Haan, J.A. Ferreira, Contribution of DG units to primary frequency control, in: International Conference on Future Power Systems, 2005, p. 6.
[6] C. Wang, M.H. Nehrir, Load transient mitigation for stand-alone fuel cell power generation systems, IEEE Trans. Energy Convers. 22 (4) (2007) 864–872.
[7] P. Thounthong, S. Rael, B. Davat, Control algorithm of fuel cell and batteries for distributed generation system, IEEE Trans. Energy Convers. 23 (1) (2008) 148–155.
[8] K.P. Adzakpa, K. Agbossou, Y. Dube, M. Dostie, M. Fournier, A. Poulin, PEM fuel cells modeling and analysis through current and voltage transient behaviors, IEEE Trans. Energy Convers. 23 (2) (2008) 581–591.
[9] J.T. Pukrushpan, A.G. Stefanopoulou, H. Peng, Control of Fuel Cell Power Systems: Principles, Modeling, Analysis and Feedback Design, Springer, USA, 2004.
[10] S. Kyung-Won, A.G Stefanopoulou, Coordination of converter and fuel cell controllers, in: Proceedings of the 13th Mediterranean Conference on Control and Automation, Limassol, Cyprus, 2005, pp. 563–568.
[11] S.-Y. Choe, J.-W. Ahn, J.-G. Lee, S.-H. Baek, Dynamic simulator for a PEM fuel cell system with a PWM DC/DC converter, IEEE Trans. Energy Convers. 23 (2) (2008) 669–680.
[12] Mohan, Undeland, Robbins, Power Electronics: Converters, Applications and Design, third ed., Wiley, USA, 2003.
[13] J. Morren, S.W.H. de Haan, J.A. Ferreira, Contribution of DG units to voltage control: active and reactive power limitations, PowerTech IEEE, Russia (2005) 1–7.